Journal of Solid State Chemistry 182 (2009) 942–947

Contents lists available at ScienceDirect

Journal of Solid State Chemistry

journal homepage: www.elsevier.com/locate/jssc

The solubility of Co in TiO_2 anatase and rutile and its effect on the magnetic properties

Meike Fleischhammer, Martin Panthöfer, Wolfgang Tremel *

Institut für Anorganische Chemie und Analytische Chemie, Johannes Gutenberg-Universität Mainz, Duesbergweg 10-14, 55099 Mainz, Germany

ARTICLE INFO

Article history:
Received 31 March 2008
Received in revised form
13 January 2009
Accepted 15 January 2009
Available online 21 January 2009

Keywords:
TiO_2
Ferromagnetism
Co doping

ABSTRACT

Co-doped anatase and rutile bulk-samples prepared by the sol–gel technique are found to be paramagnetic at room-temperature. Only further annealing in Ar/H_2 gas results in a ferromagnetic behavior. X-ray diffraction and electron-microscope studies reveal for low doping levels $<4\%$ the formation of Co-doped rutile samples and the formation of $CoTiO_3$ as a new phase. Co_3O_4 can be detected in anatase samples with Co doping levels $\geqslant 4\%$. The observed Co oxides are reduced by Ar/H_2 to Co metal. The room-temperature ferromagnetism can therefore be traced back to a segregation of metallic Co.

1. Introduction

Co-doped TiO_2 was considered to belong to the class of diluted magnetic oxides (DMO) after thin film samples of Co-doped anatase and rutile were reported to exhibit ferromagnetic behavior at room-temperature [1,2]. However, besides the preparation of such samples by means of oxygen plasma assisted molecular beam epitaxy (OPA-MBE) [3,4], pulsed laser deposition (PLD) [1,5–7], and reactive co-sputtering [8–10] techniques, the reported results are quite contradictory. In particular, the chemical nature of the ferromagnetic phase is subject to discussion. Since most of the above film synthesis methods were performed under vacuum or low oxygen conditions, the occurrence of metallic cobalt clusters as the origin of the ferromagnetism must be considered. In fact Kim et al. [5] and Murakami et al. [11] found metallic cobalt in their samples. Also the variation of the oxygen partial pressure during the synthesis of Co-doped TiO_2 leads to significant changes of the magnetic properties [5,12].

The significant discrepancies in the results reported on doped TiO_2 films in different studies is complicated furthermore by crystal chemical considerations that question the solubility of Co in TiO_2. Considering the differences of the ionic radii of 23% between Co^{2+} (76 pm [13]) and Ti^{4+} (61 pm [13]), a substitution of Ti^{4+} by Co^{2+} is less feasible. Additionally, the differences of the valence state between Ti^{4+} and Co^{2+} either require the creation of oxygen-holes (v^{2-}) or an interstitial substitution (Co^{2+}_{int}) according:

$$Ti^{4+} = Co^{2+} + v^{2-}$$

$$Ti^{4+} = Co^{2+}_{sub} + Co^{2+}_{int}$$

In the former case a structural rearrangement to a Magnéli type phase (Ti_nO_{2n-1}, $4 \leqslant n \geqslant 9$) [14] may be expected at a doping rate of 10 at% Co or higher, which has not been observed so far.

One may still think of stuffing voids in the corresponding TiO_2 host lattices, i.e. the highly distorted octahedral void at $(0\,\frac{1}{2}\,\frac{1}{2})$ and the highly distorted tetrahedral voids at $(0.155\,0.115\,\frac{1}{2})$ in the rutile structure type. Even in case of Co^{3+} those are too small, in particular when taking into account the exclusive preference of Co^{3+} to octahedral coordination.

It is unclear, whether the discrepancies between the theoretical considerations that appear to limit the Co solubility and the partially contradictory results of the previous experimental studies are due to different experimental techniques used, including the particular characteristics of thin films (REF), or to analytical difficulties caused by small sample volumes. To answer these questions, a systematic study of the Co solubility in TiO_2 is needed. Here, we present a detailed experimental investigation of the Co solubility in TiO_2 bulk samples. The advantage of the present approach is an easily reproducible synthesis technique that avoids a complex interplay between substrate and thin film, and thus provides more general results. In addition, large sample volumes allow a more detailed analysis of the phase equilibria and the magnetic bulk properties of the doped samples. These results can therefore provide a basis for the interpretation and re-evaluation of previous thin-film and nano-scale studies.

* Corresponding author. Fax: +49 6131 39 25135.
E-mail address: tremel@uni-mainz.de (W. Tremel).

0022-4596/$ - see front matter © 2009 Elsevier Inc. All rights reserved.
doi:10.1016/j.jssc.2009.01.011

2. Experimental

2.1. Synthesis

The Co-doped TiO_2 samples are prepared by a sol-gel method. Ethanolic solutions of $CoCl_2 \times 6H_2O$ and Titanium(IV)-isopropoxide were mixed in varying ratios. The hydrolysis is started by addition of a small amount of hydrochloric acid solution (pH = 3). All gels prepared looked visually homogeneous concerning color as well as turbidity pointing towards a homogeneous distribution of the different cations in the gels. Further details are reported elsewhere [15]. The gels were annealed in air at 400 and 800 °C in order to obtain Co-doped anatase and rutile samples, respectively. Afterwards a part of the samples were annealed again in a H_2/argon atmosphere.

2.2. Characterization

The X-ray diffraction patterns for identification of the several phases in the samples were recorded with a Bruker D8 X-ray diffractometer with Cu$K\alpha$ radiation in reflection geometry. The lattice parameters were refined by means of LeBail fits using Jana 2000 [16].

For the microprobe (MEMS) and scanning electron microscope (SEM) analysis the samples were embedded in epoxy resin, ground and polished. The measurements to obtain microprobe backscattered electron (BSE) images were performed with a JEOL JXA-8200 (15 kV) microprobe and a LEO 1530 (6 kV) scanning electron microscope operating either in wavelength dispersive X-ray (WDX) or energy dispersive X-ray (EDX) mode. Operating conditions were an accelerating voltage of 15 kV, a beam current of 20 mA and 10 s counting time for all elements. The electron microprobe diameter was ~0.5 μm. A matrix correction program was applied to the raw data. Synthetic oxide or mineral standards were used for calibration. The element concentration traverses through sample grains were performed as a check for homogeneity.

The magnetic measurements were performed with a Quantum Design MPMS-XL-5 (SQUID) at 300 K between 40 and −40 kOe and at 5 kOe between 300 and 5 K. The susceptibility including the diamagnetic correction was calculated according to: $\chi = (M_m/H) + 0.0000142\ mol^{-1}$ [17].

3. Results and discussion

3.1. Structural characterization

The X-ray diffraction patterns (Fig. 1a) of the Co-doped samples annealed at 800 °C show reflections corresponding to rutile ($P4_2/mnm$, $a = 4.594$ Å, $c = 2.959$ Å) plus further reflections. These can clearly be assigned to the Ilmenite-type $CoTiO_3$. This means that the doping with Co does not result in a substitution of Co into rutile. In addition, the lattice parameters of the rutile phase in these samples do not exhibit any dependence on the cobalt concentration (Fig. 2). As expected, annealing of the Co-doped rutile samples in a H_2/argon atmosphere leads the formation of β-Co (Fig. 1b).

In the case of the samples annealed at 400 °C and a Co doping <6 at% the X-ray diffraction patterns (Fig. 3a) exclusively exhibit reflections corresponding to anatase ($I4_1/amd$, $a = 3.7886$ Å,

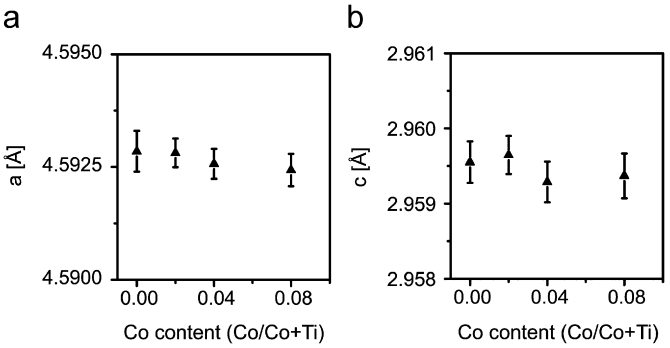

Fig. 2. Lattice parameters a and c of 0–8 at% Co-doped rutile. The error bar is equivalent to 3σ.

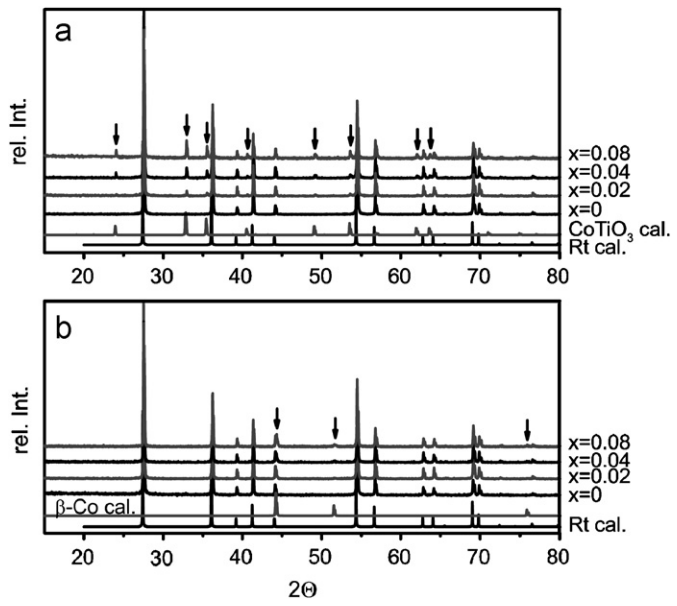

Fig. 1. X-ray diffraction pattern of 0–8 at% Co-doped TiO_2 samples after annealing at (a) 800 °C and (b) further annealing in H_2/argon. Arrows mark the reflections of the second phase corresponding to the calculated patterns of ilmenite ($CoTiO_3$) and Co metal (ß-Co). Also the calculated pattern of rutile (Rt) is shown.

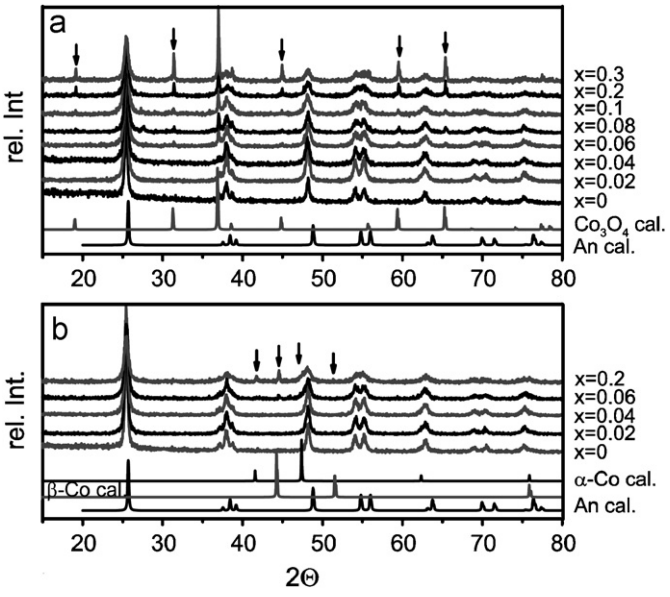

Fig. 3. X-ray diffraction pattern of 0–20 at% Co-doped TiO_2 sample after annealing at (a) 400 °C and (b) further annealing in H_2/argon. Arrows mark the reflections of the second phase corresponding to the calculated patterns of spinel (Co_3O_4) and Co metal (ß-Co and α-Co). Furthermore, the calculated pattern of anatase (An) is shown.

$c = 9.507$ Å). At 6 at% Co additional reflections due to Co_3O_4 emerge. After annealing in H_2/argon atmosphere the patterns of Co-doped anatase samples with Co <6 at% exhibit no change (Fig. 3b). In contrast, the diffraction patterns of the higher doped samples exhibit reflections of α-Co and β-Co after annealing in H_2/argon atmosphere. This suggests a substitution of Ti by Co of up to 6 at% anatase. Due to the larger ionic radius of the Co^{2+} cation, a substitution of Ti^{4+} by Co^{2+} should be associated with a significant change of the lattice parameters. Yet, the refined lattice parameters of the anatase phase do not vary within the 3σ range upon Co-doping (Fig. 4). This indicates toward a very low solubility of Co in anatase TiO_2.

3.2. Chemical and morphological characterization

The BSE images of the Co-doped rutile samples show square-edged crystals embedded in a fine grained basic matrix. The crystals are interspersed with bright inclusions (Fig. 5). The determination of the chemical composition with the SEM-EDX and the microprobe reports a distinct enrichment of Co in the inclusions (Table 1).

The Co-doped anatase samples show a similar microstructure as the rutile samples, but the crystals of the anatase samples exhibit only few bright inclusions. Instead there are clefts in the crystals, and the basic matrix is filled up with light material (Fig. 6). The EDX and WDX measurements of an anatase sample doped with 4 at% Co exhibit at most 3.1–3.5 at% Co in the homogeneous parts. Further increase of the bulk Co content does not result in an increased Co content in the homogeneous parts of the crystals (Table 1). Yet, Co is enriched in the clefs. This finding is represented as well by an element mapping experiment of a 4 at% doped anatase sample (Fig. 7). Therefore, the Co solubility in anatase must be lower than 4 at%.

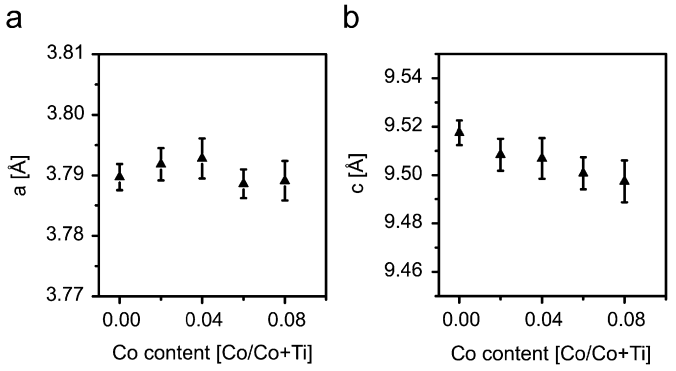

Fig. 4. Lattice parameters a and c of 0–8 at% Co-doped anatase. The error bar is equivalent to 3σ.

3.3. Magnetic properties

Fig. 8a shows the field and temperature variations of the magnetization for the Co-doped rutile samples. All samples are

Table 1
Co content [Co/Co+Ti] determined from the EDX-measurements of (a) Co-doped anatase and (b) Co-doped rutile.

x	Homogeneous parts	Clefts	Inclusions
(a) Anatase			
0.04	0.031–0.043	0.032–0.08	0.04
0.06	0.047–0.7	0.103–0.247	0.049–0.07
0.1	0.048–0.079	0.067–0.381	–
(b) Rutile			
0.04	0.014–0.039	–	0.045–0.203
0.08	0.029–0.088	–	0.042–0.228

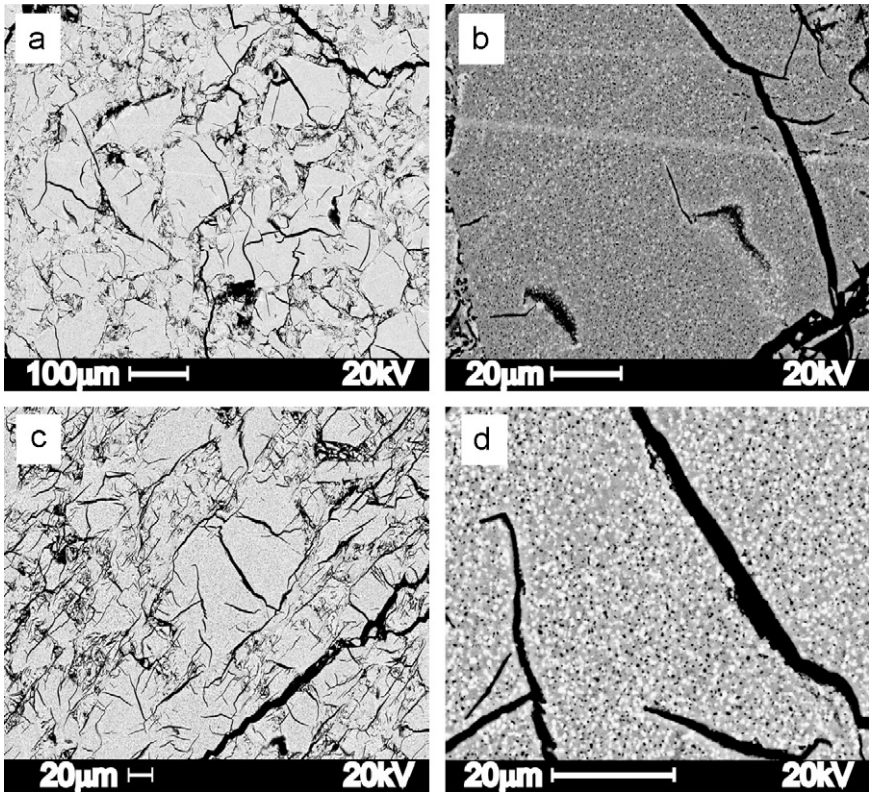

Fig. 5. BSE pictures of a rutile-sample doped with 4 at% Co (a, b) and 8 at% Co (c, d).

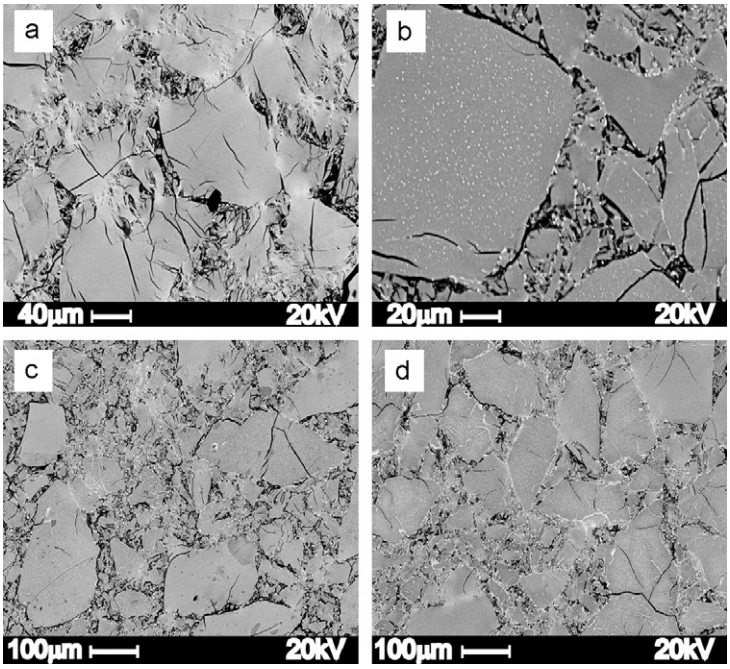

Fig. 6. BSE pictures of anatase sample doped with 4 at% Co (a, b), 6 at% Co (c) and 10 at% Co (d).

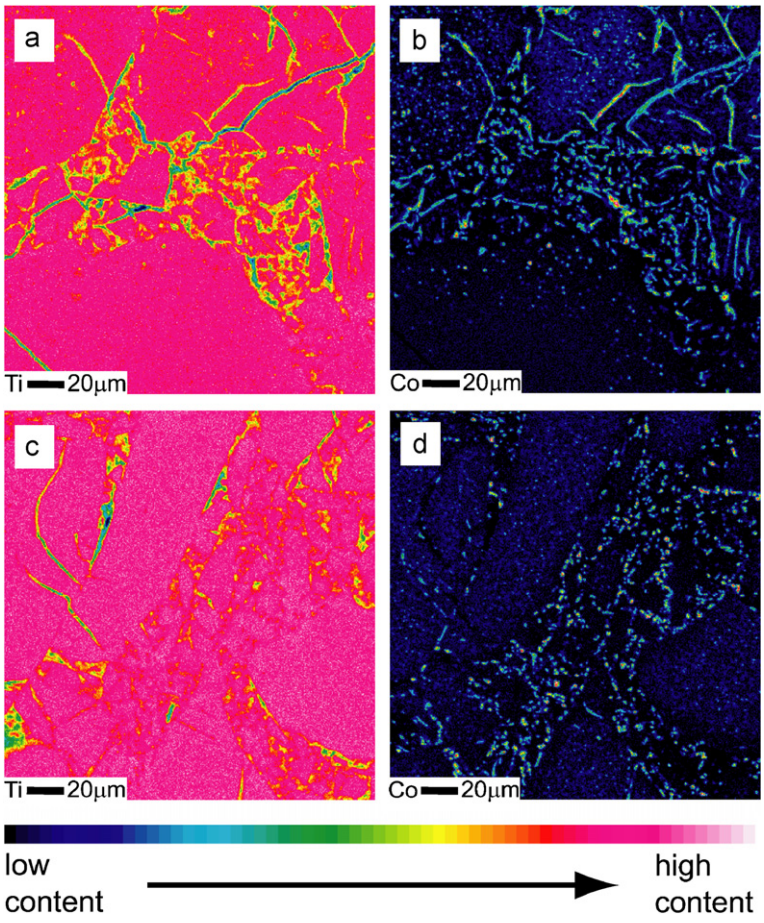

Fig. 7. Element mapping experiment of (a) Ti and (b) Co in a 4 at% Co-doped anatase sample, (c) Ti and (d) Co in a 6 at% Co-doped anatase sample.

paramagnetic at room temperature. The $1/\chi$ vs. T plot (Fig. 9a) shows a Curie–Weiss behavior between 300 and 38 K. At 38 K an antiferromagnetic transition occurs. The antiferromagnetic transition temperature corresponds to the Néel temperature of $CoTiO_3$ [18]. According to the formation of metallic Co during the annealing in H_2/argon, the reduced Co-doped rutile samples are ferromagnetic (Fig. 8b) with a saturation magnetization of $M_S = 1.8\ \mu_B$/Co.

The doped anatase samples also exhibit paramagnetic behavior at room temperature (Fig. 10a). The antiferromagnetic transition of Co_3O_4 ($T_N = 33$ K [19]), which was detected for the $\geqslant 4$ at% Co-doped samples, is exclusively observable in the very heavily doped samples (Fig. 11). After annealing in H_2/argon atmosphere the anatase samples are ferromagnetic for Co-contents $\geqslant 4$ at% (Fig. 10b). The 2 at% Co sample remains paramagnetic. The saturation magnetization increases upon increasing the Co-content (4 at%: 0.07 μ_B/Co, 6 at%: 1.03 μ_B/Co, 20 at%: 1.26μ_B/Co). If Co metal, which was detected in the $\geqslant 6$ at% Co-doped anatase samples, were the origin of the ferromagnetism, the saturation magnetization should be 1.8 μ_B/Co for all samples. Furthermore, the temperature dependent magnetic measurements exhibit an anomalous depression between 300 and 50 K (Fig. 12), which clearly departs from the magnetic behavior of Co metal. A possible explication could be the presence of a third, antiferromagnetic phase with $T_N \approx 300$ K besides metallic Co and TiO_2, i.e. CoO ($T_N = 293$ K [20]).

The magnetic behavior of the 2 at% Co-doped anatase sample does not change after reduction. This may be an important evidence for the incorporation of Co^{2+} into anatase, preventing the reduction to metallic Cobalt in H_2/argon atmosphere.

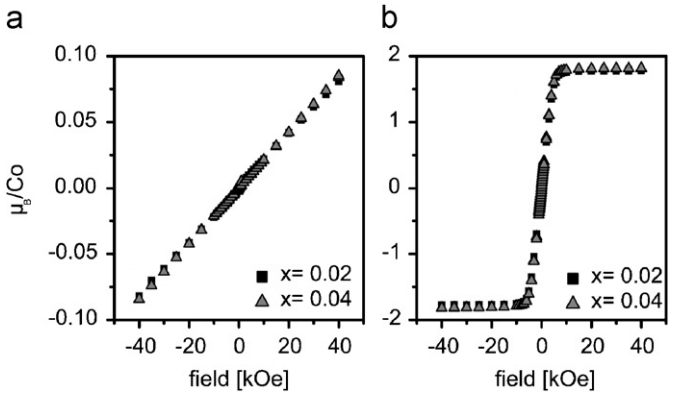

Fig. 8. Magnetization vs. magnetic field at 300 K of 2% Co-doped (black square) and 4% Co-doped (triangle) rutile samples annealed in (a) air and (b) H_2/argon.

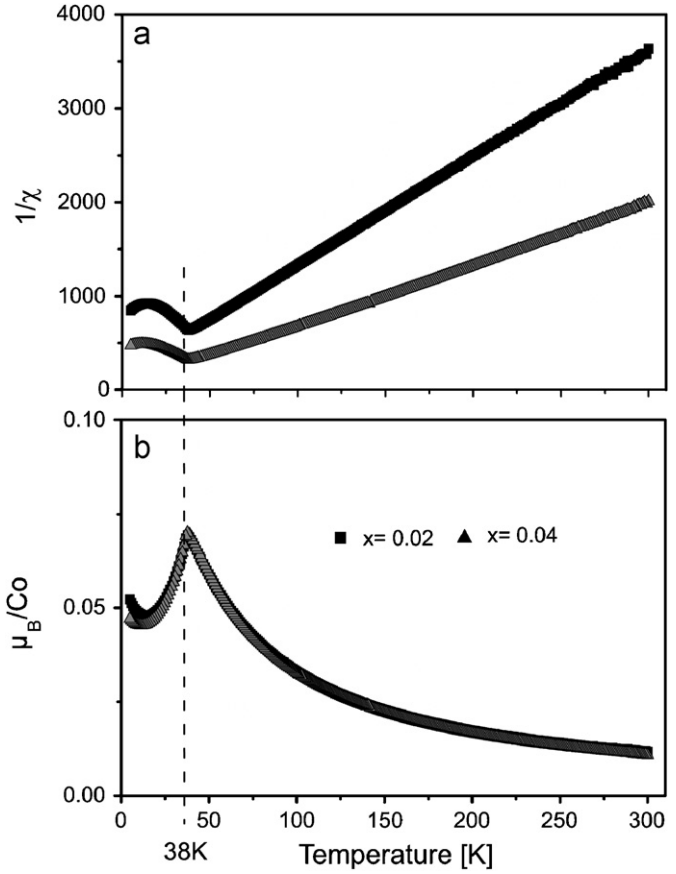

Fig. 9. Magnetization (b) and susceptibility (a) vs. temperature at 5 kOe of 2% Co-doped (black square) and 4% Co-doped (triangle) rutile samples annealed in air.

4. Conclusions

The doping of rutile with Co does not lead to a homogeneous $Co_xTi_{1-x}O_{2-y}$ rutile phase. Instead the rutile crystals show inclusions of ilmenite $CoTiO_3$ above a minimum doping of 2 at% Co as shown by means of X-ray diffraction and temperature dependent magnetic measurements. Due to the presence of $CoTiO_3$ besides rutile, annealing of the samples in H_2/argon atmosphere leads to the reduction of $CoTiO_3$ and formation of metallic Co. The observed room-temperature ferromagnetism of the reduced Co-doped rutile samples is clearly caused by the presence Co metal clusters. These results strongly indicate that Co is not incorporated in the rutile structure.

The doping of anatase with $\geqslant 4$ at% Co leads to the formation of a mixture of anatase and antiferromagnetic Co_3O_4. After annealing these samples in H_2/argon atmosphere, the magnetic behavior

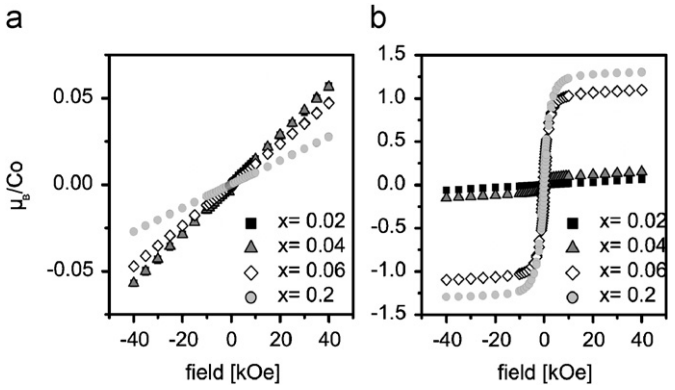

Fig. 10. Magnetization vs. magnetic field at 300 K of 2% Co-doped (black square) and 4% Co-doped (triangle) anatase samples annealed in (a) air and (b) H_2/argon.

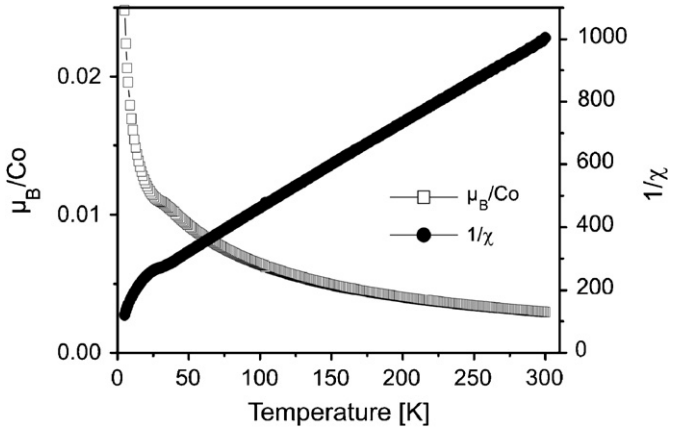

Fig. 11. Magnetization (μ_B/Co) and susceptibility ($1/\chi$) vs. temperature at 5 kOe of 20% Co-doped anatase samples annealed in air.

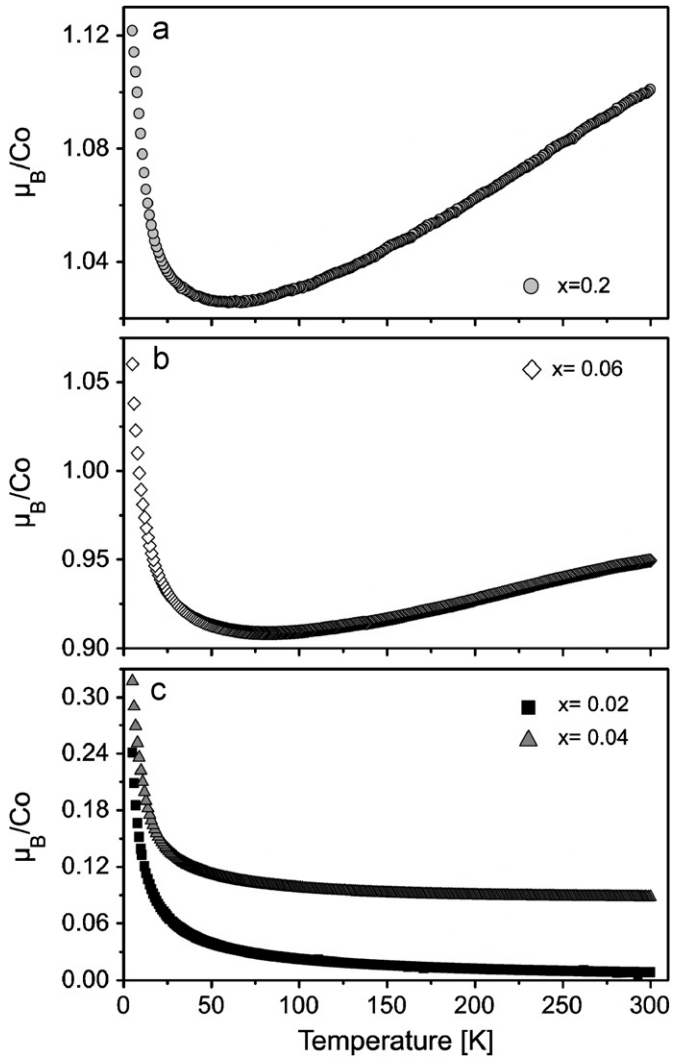

Fig. 12. Magnetization vs. temperature at 5 kOe of (c) 2% Co-doped (black square) and 4% Co-doped (triangle), (b) 6% Co-doped and (a) 20% Co-doped anatase samples annealed in H_2/argon.

also changes from paramagnetic (antiferromagnetic) to ferromagnetic due to formation of Co metal and CoO.

The case of $a<4$ at% doping is not fully resolved. In the low doped anatase samples no evidence was found for other phases beside anatase or inhomogeneities. Furthermore the paramagnetism of the sample is unaffected by annealing in H_2/argon atmosphere; therefore we can assume the limit of solubility of Co^{2+} in TiO_2 anatase lies between 2 and 4 at%.

The experimental studies of this works clearly exclude the possibility of substitution of Ti^{4+} by Co^{2+} in TiO_2. The reports about ferromagnetic Co-doped TiO_2 films and nanosamples could possibly be explained by an overlooked second phase. However, the influence of the substrate used for preparing films may be an important factor in the formation and properties of these films [1,2]. Based on this work we cannot exclude the possibility of a forced Co-substitution aided by a suitable substrate. This might be a goal of future research.

Acknowledgments

We acknowledge the help of Dr. Burkhard Schulz-Dobrick for microprobe analysis and Dr. N. P. Walter for SEM measurements.

References

[1] Y. Matsumoto, Science 294 (2001) 1003.
[2] Y. Matsumoto, R. Takahashi, M. Murakami, T. Koida, X.J. Fan, T. Hasegawa, T. Fukumura, M. Kawasaki, S.Y. Koshihara, H. Koinuma, Jpn. J. Appl. Phys. Part 2 40 (2001) L1204.
[3] S.A. Chambers, S. Thevuthasan, R.F.C. Farrow, R.F. Marks, J.U. Thiele, L. Folks, M.G. Samant, A.J. Kellock, N. Ruzycki, D.L. Ederer, U. Diebold, Appl. Phys. Lett. 79 (2001) 3467.
[4] T.C. Kaspar, T. Droubay, C.M. Wang, S.M. Heald, A.S. Lea, S.A. Chambers, J. Appl. Phys. 97 (2005) 073511.
[5] D.H. Kim, J.S. Yang, K.W. Lee, S.D. Bu, T.W. Noh, S.J. Oh, Y.W. Kim, J.S. Chung, H. Tanaka, H.Y. Lee, T. Kawai, Appl. Phys. Lett. 81 (2002) 2421.
[6] Y. Yamada, H. Toyosaki, A. Tsukazaki, T. Fukumura, K. Tamura, Y. Segawa, K. Nakajima, T. Aoyama, T. Chikyow, T. Hasegawa, H. Koinuma, M. Kawasaki, J. Appl. Phys. 96 (2004) 5097.
[7] J. Li, O.H. Sow, S.X. Rao, C.K. Ong, D.N. Zheng, Eur. Phys. J. B 32 (2003) 471.
[8] W.K. Park, R.J. Ortega-Hertogs, J.S. Moodera, A. Punnoose, M.S. Seehra, J. Appl. Phys. 91 (2002) 8093.
[9] A. Punnoose, M.S. Seehra, W.K. Park, J.S. Moodera, J. Appl. Phys. 93 (2003) 7867.
[10] D.H. Kim, J.S. Yang, K.W. Lee, S.D. Bu, D.W. Kim, T.W. Noh, S.J. Oh, Y.W. Kim, J.S. Chung, H. Tanaka, H.Y. Lee, T. Kawai, J.Y. Won, S.H. Park, J.C. Lee, J. Appl. Phys. 93 (2003) 6125.
[11] M. Murakami, Y. Matsumoto, T. Hasegawa, P. Ahmet, K. Nakajima, T. Chikyow, H. Ofuchi, I. Nakai, H. Koinuma, J. Appl. Phys. 95 (2004) 5330.
[12] A. Manivannan, G. Glaspell, M.S. Seehra, J. Appl. Phys. 94 (2003) 6994.
[13] R.D. Shannon, Acta Crystallogr. A 32 (1976) 751.
[14] S. Andersson, B. Collén, U. Kuylenstierna, A. Magnali, Acta Chem. Scand. 10 (1957) 1641.
[15] M. Fleischhammer, Ph.D. Thesis, University of Mainz, 2006.
[16] V. Petricek, M. Dusek, L. Palatinus, The Crystallographic Computing System, Institute of Physics, Praha, Czech Republic, 2000.
[17] W. Haberditzl, Magnetochemie, Akademie-Verlag, Berlin, 1968.
[18] R.E. Newnham, J.H. Fang, R.P. Santoro, Acta Cryst. 17 (1964) 240.
[19] W. Kündig, M. Kobelt, H. Appel, G. Constabaris, R.H. Lindquist, J. Phys. Chem. Solids 30 (1969) 819.
[20] C. Shull, W. Strauser, E. Wollan, Phys. Rev. 83 (1951) 333.